JOINT EUROPEAN TORUS JET

JET–P(93)79

M.F.F. Nave, S. Ali-Arshad, B. Alper, B. Balet, D. Borba,
C.D. Challis, H.J. de Blank, M. von Hellermann, T.C. Hender,
G.T.A. Huysmans, W. Kerner, G. Kramer, F. Porcelli, J. O'Rourke,
L. Porte, G. Sadler, P. Smeulders, A.C.C. Sips, P.M. Stubberfield,
D. Stork, R. Reichle, J. Wesson, W. Zwingmann.

MHD Activity in JET Hot Ion H-Mode Discharges

MHD Activity in JET Hot Ion H-Mode Discharges

M.F.F. Nave[1], S. Ali-Arshad, B. Alper, B. Balet, D. Borba, C.D. Challis, H.J. de Blank, M. von Hellermann, T.C. Hender[2], G.T.A. Huysmans, W. Kerner, G. Kramer, F. Porcelli, J. O'Rourke, L. Porte, G. Sadler, P. Smeulders, A.C.C. Sips, P.M. Stubberfield, D. Stork, R. Reichle, J. Wesson, W. Zwingmann.

JET-Joint Undertaking, Culham Science Centre, OX14 3DB, Abingdon, UK

[1]Associacao EURATOM/1ST, Instituto Superior Tecnico, Lisbon, Portugal.
[2]AEA Technology, Fusion, Culham, Abingdon, Oxon, OX 14 3DB, UK.

Preprint of a paper to be submitted for publication in
Nuclear Fusion
December 1993

ABSTRACT

The MHD effects observed in the hot-ion H-modes, including those generated in the Preliminary Tritium Experiment, are described. Some observations were found to be similar to those in high beta regimes, while others are new and appear to be pertinent to high performance discharges only. The high performance phase is largely sawtooth-free and dominated by fishbone activity, which increases in amplitude throughout this phase. During termination of the high performance phase, the growth of a large variety of MHD activity with low mode numbers is observed. Also, edge instabilities possibly associated with much larger mode numbers are seen in the D_α emission. In some cases the unusual structure of two central m=n=1 islands was found. Resistive MHD modelling indicates a nearly flat, non-monotonic q-profile. In many discharges a sawtooth collapse with an extremely fast heat-wave, immediately followed by an ELM is observed at, or shortly following, the termination of the high performance.

I - INTRODUCTION

The hot-ion H-mode regime has produced the highest performance plasmas so far achieved in the JET Tokamak [1]. This regime combines the occurrence of the H-mode with bulk plasmas where the ion temperature is significantly higher than the electron temperature (T_i>1.5 T_e). The resulting plasmas show the highest neutron yields obtained in pure deuterium (D-D) JET discharges. Plasmas of this type were used in the Preliminary Tritium Experiment (PTE) in which the JET device operated the world's first plasmas with significant tritium content (90%D:10%T) [2].

The best of the JET hot-ion H-modes in D-D offer a predicted fusion amplification factor (Q_{DT}) of around unity for a 50:50 D-T discharge. A series of publications has already discussed different aspects of the JET PTE plasmas [1-4]. A description of the particle and energy transport in the PTE discharges and in the deuterium hot-ion H-modes used in their development is found in the paper of Balet et al [5]; whilst a detailed phenomenology and the possible reasons for termination of the high performance phase of these plasmas are to be covered by Reichle et al. [6]. The present paper concentrates on the MHD effects observed in the hot-ion H-modes (including those generated in the PTE), the aim being to present details of the MHD phenomena in the context of the observed changes in plasma performance.

The systematics of this MHD behaviour are contrasted with previous JET experiments which have produced regimes with toroidal beta values, β_ϕ, close to the Troyon limit [7,8]. Specifically, these regimes had values of toroidal beta normalised to the Troyon limit [9] (β_T=2.8 I(MA)/a(m)B_ϕ(T)) given by $\beta_N=\beta_\phi/\beta_T$ ~1-1.2. They were generated principally by using Neutral Beam Injection (NBI) heating at low toroidal fields ($B_\phi \leq 1.2$T) and low plasma currents (I_p=1.5-2.0 MA). The high-β plasmas were generally characterised by $T_i \sim T_e$, although some hot-ion plasmas were obtained [8]. Although the good confinement phase of the hot-ion H-modes spanned a wide range of beta values [5] all with $\beta_N<0.9$, many of the MHD observations were typical of observations in high-β discharges closer to the Troyon limit. In order to understand the relevance of beta effects in the decline of the good confinement, the MHD observations, and in particular the characteristics of sawtooth crashes, will be described with respect to β_N.

In section II we present an overview of the MHD observations in a subset of hot ion H-mode discharges with plasma current I_p=3 MA and toroidal field in the range B_ϕ=2.6-3.1 T. The subsequent sections, III-VII will discuss effects related to individual types of MHD activity. The results of modelling of the observations will be presented in section VIII.

II - DISCHARGE OVERVIEW

In the following we will refer to three confinement phases that characterise these discharges: (I) the good confinement phase, when the thermal confinement is nearly twice the ITERH92-P value [5], (II) the termination phase, defined here as starting when the total neutron flux starts to decline (either slowly or in a sudden crash) and finishing with a large influx of impurities, and (III) a subsequent poorer confinement phase, with the H-mode retained but having lost the hot ion characteristics. From the point of view of MHD observations this subdivision is not arbitrary, as different phenomena have actually been observed in each phase.

Fig 1 gives an overview of the temporal evolution of the plasma energy and the total neutron rate together with low n magnetic perturbations, ELM and sawtooth activity, for three hot-ion H-mode discharges: discharge 26148 with 10% tritium, the best D-D discharge, no. 26087, and discharge 26095, which had a minute quantity (0.07%) of tritium. These three discharges are discussed in detail in reference [5]. The general aspects described here are common to both the D-D and D-T discharges.

The shaded areas in Fig 1 indicate phase I, i. e. the high confinement phase. The Fig shows that phase I is preceded by small amplitude edge localised modes (ELMs) , indicated by the sudden spikes in the D_α and the ECE signals. Phase I is a period nearly free of ELMs and of sawtooth collapses. However, unlike previously reported observations in sawtooth-free regimes [10] this is not a period of low MHD activity. The magnetic fluctuation traces in Fig 1 show the root mean square (rms) level of magnetic activity with low toroidal mode numbers. The n=1 activity is dominant in phase I, and is generally seen to increase with increasing plasma energy and neutron emission rate. A comparison of these signals with faster magnetic data (available for shorter durations) shows that during phase I this activity is mainly fishbones. (The spikes in the n=1 signal correspond to the envelopes of fishbone bursts).

During phase I the effect of fishbone bursts is seen in the electron-cyclotron emission (ECE) and soft-X-ray (SXR) signals from the plasma core as frequent, small indentations similar to small sawteeth. Fig 2 shows a close-up of ECE signals for discharge 26148. The central signal shows the effect of fishbones. The signal near the edge also shows a sawtooth-like behaviour. This is not always correlated to fishbone activity, thus indicating that although the D_α and ECE spikes which are characteristic for the ELMs are no longer observed, the edge MHD activity is not completely stabilised.

Occasionally, a single sawtooth collapse was observed during phase I. Unlike the sawtooth collapses observed in phase II which are closely followed by ELMs, the earlier sawtooth collapses, observed before or at the beginning of phase I, are not correlated to ELMs. This is the case of the sawtooth at the beginning of phase I in discharge 26095. The sawtooth collapse is followed by a period of quiescent n=1 activity.

During the high performance phase in many discharges there seems to be a limitation to the enhanced performance as shown by a saturation in the ion temperature profiles. This is accompanied by a slowing down in the rate of increase of the central neutron rate[5,11]. Before the end of phase I, a saturation of the total neutron rate is normally observed. This can be seen in Fig 1 for discharges 26087 and 26095. In discharge 26148, however, the good confinement phase ends before the saturation of the total neutron rate is established.

A detailed description of phase II can be found in the paper of Reichle et al [6]. In over 50% of the discharges, the decline of the neutron yield coincides with a slow

temperature degradation, typically lasting a few tens of ms. This slow degradation has been labelled "the slow termination". In some of these discharges the slow temperature fall is followed by a much faster collapse due to a sawtooth combined with an ELM. In some of the remaining discharges the end of the high performance phase is sudden and occurs at the time of a catastrophic MHD event, such as a giant ELM, or a sawtooth collapse nearly always combined with an ELM. The discharges shown in Fig 1 exemplify the above types of behaviour. In discharge 26148 the collapse of the neutron yield (at β_N~0.6) is sudden and associated with a collapse of the whole temperature, caused by a sawtooth crash combined with a large ELM. In discharge 26095, the temperature collapse (at β_N~0.75) is slower and appears in conjunction with a small and slow increase in the D_α signal. Discharge 26087 shows a combination of both slow and fast behaviours, i.e. a slower temperature degradation with a small increase of D_α (at β_N~0.8) is followed by a fast sawtooth-like crash combined with an ELM.

At the start of phase III the impurity content is largely increased which makes the collapse of the neutron yield irreversible [5-6]. (The central SXR signal in Fig 3, shows a sudden increase in emission immediately following the sawtooth/ELM event which is caused by an influx of impurities). In the discharges where phase II is terminated by a sawtooth, n=3 activity is observed to grow for a few hundred milliseconds after the collapse. This is clearly seen in Fig 1 for discharges 26087 and 26148. This phase is also characterised by the appearance of large ELMs.

IIa- MODE IDENTIFICATION

The slow rms signals shown in Fig 1 were available throughout the discharges giving a first indication whether MHD activity is significant. However, the precise identification of the MHD modes observed in each phase and their amplitudes can only be obtained after careful analysis of data taken with a fast time resolution. In low density, NBI heated discharges, the central plasma rotation varies linearly with the ion temperature [12,13]. For the high T_i values, >20keV, reached during the hot-ion H-mode regimes, central plasma rotations frequencies of ~25 kHz were observed. The sampling frequency of most diagnostics was limited and this put a limit on the modes which could be identified. In addition, limits on the data storage capacity of the diagnostic data acquisition memories placed a restriction on the time windows which could be analysed in detail, a full picture could thus not emerge from consideration of only one discharge.

The mode analysis presented below has been obtained from magnetic pick-up coils, microwave reflectometer, and soft X-rays (SXR) signals, which give limited frequency information up to 120 kHz. (For a description of JET diagnostics see references [14, 14a]). Storage of fast SXR data was triggered at the sawtooth collapses, which allowed us a detailed study of both the toroidal and poloidal spatial structure of oscillations in the 4ms preceding the sawtooth. However, similar SXR analysis is missing at most other times of interest.

Fig 3 gives an analysis of fast magnetic data for discharge 26087. It shows two distinct n=1 oscillations with frequencies close to the plasma rotation frequency of the q=1 radius. In accordance with hybrid two fluid-kinetic models which predict two branches for the m=n=1 mode [15], we will refer to the faster oscillation as the fishbone mode and to the slower one as the "internal kink" mode. The slower m=n=1 oscillation is the precursor to the sawtooth collapse, and in some discharges it is not observed until phase II, from 0.2 to a few ms before a sawtooth crash.

Slower n=1, and occasionally n=2, oscillations, corresponding to magnetic islands with low poloidal numbers, m>1, were observed further out in some discharges during phase I. Fig 4a gives the Fourier spectra of a fast magnetic signal measured during phase I for discharge 26095. The mode with largest amplitude at 24 kHz corresponds to fishbone activity. The lower frequency mode, at 9.5kHz, has toroidal mode number n=2. Its amplitude is too low to allow a determination of the poloidal mode number. Fig 4b shows the profile of plasma rotation from charge exchange measurements. A comparison of the observed mode frequency to the ratio of the toroidal mode number with the plasma rotation frequency, indicates that the lower frequency mode originates within the outer 30% of the plasma.

Like the "internal kink", these outer modes were only observed to grow significantly during phase II, which as it will be seen in the following sections, is a phase showing a complex variety of modes.

III - FISHBONES

A detailed description of fishbone activity in JET discharges can be found in reference [16]. These are m=n=1 oscillations which are often observed in auxiliary heated JET plasmas by magnetic, SXR and ECE diagnostics . They may appear either in bursts or in continuous form. In the discharges discussed here, as in most other JET discharges no effect of individual fishbone bursts on the total neutron emission is

observed, indicating that changes in the total neutron emission associated with each burst are <5% (the noise level). Nevertheless, fishbone oscillations can be clearly distinguished from other m=n=1 oscillations which are sometimes observed simultaneously (as shown in Fig 3) by the higher frequency. In the hot-ion H mode discharges fishbones are the most prominent MHD activity observed in phase I.

As mentioned previously, a common feature observed during phase I is the saturation of the bulk ion temperature and the associated saturation of the central neutron emission rate. These changes in T_i and the central neutron rate in most discharges are observed at or shortly after the onset of fishbones. Also, shortly after the onset of fishbones a gradual slowing down in the rate of increase of T_e in the inner region of the plasma starts to be observed.

Fig 5 shows that for discharge 26095, a slowing down in the rates of increase of T_i, T_e and the central neutron emission start very early, around 12.5s. These effects are interrupted by a sawtooth crash at t=12.8s, which also brings down the level of n=1 activity. A second sudden change in the slopes of T_i and of the central neutron rate occurs at 13.2s. This is followed by a gradual slowing down in the rate of increase of the central T_e. These described effects occur near the time when fishbone bursts start to be observed in the magnetic signals both before and after the sawtooth collapse. The spikes in the slow magnetic signal shown in Fig 5 correspond to the envelopes of fishbone bursts (Except for the spike at the collapse of the neutron yield, which also corresponds to the growth of n=2 activity.).

Transport calculations reported in [5], where the T_i profile is used as an input parameter, have shown that the change of slope of the central neutron emission can be accounted for by the time evolution of the measured ion temperature profile. These simulations contained no modelling of MHD effects, and the cause of the halt in the rise of the ion temperature profile remains to be explained. As fishbones are present at the time when these changes occur, the magnetic reconnection associated with these modes is likely to have some effect on thermal confinement although how significant this is, is still an open question. Fishbones could also contribute indirectly by redistributing the fast ions in the core of the plasma. The effect of fishbones will depend both on the amplitude and the repetition rate of the bursts.

Fishbones are normally observed on the central electron temperature as frequent, small drops in T_e similar to small sawteeth. In JET low beta discharges the displacement of the core associated to a single burst is small, typically 2-4 cm. The

effect around q=1 is normally the largest, where flattenings of the SXR and ECE profiles as large as 10 cm have been observed [16]. In low B_ϕ discharges near the Troyon limit, SXR observations showed little difference between fishbone and sawtooth effects [16], with core displacements around 30cm and probably island sizes approaching similar magnitudes. Due to limitation of the data it is difficult to measure the island sizes in the discharges discussed here. For the intermediate β_N observed during the good performance phase and intermediate fishbone amplitudes, we expect the fishbone effects on the profiles to be in between those two cases mentioned. For discharge 26095, at the time when the total neutron rate saturates, displacements of 15-17 cm were obtained from SXR data.

Typically the time of separation between fishbone bursts in the discharges discussed here is very short, <4ms. Fig 3 shows that the fishbones observed in discharge 26087 are almost a continuous mode, implying that an m=n=1 island is always present. The island size, although increasing and decreasing at periodic intervals, is on average growing. In some discharges the fishbone bursts turn into a completely continuous mode at the end of phase I An example of this change in the character of the fishbone activity close to the end of the high performance phase is shown in section V below.

Fast data shows that the duration of the fishbone bursts can be short enough to be comparable to the smoothing time in the rms magnetic signals. This can lead to an underestimate of the peak amplitude by as much as 30% for the short lived bursts. Since, in the absence of fast data, the precise duration and shape of bursts is unknown, the rms traces should be considered with a 30% margin of error for fishbone activity. Within this error, the amplitude of the fishbones in the 3 discharges shown in Fig 1 and in several other cases was found to reach similar values at the end of phase I.

IV - SAWTEETH

The characteristics of temperature collapses just before or at the beginning of the good confinement phase were compared to the temperature crashes in phase II. This gave a range of β_N from 0.2 to 0.8. Within those values two types of temperature collapses were found: a) fast sawtooth-like collapse, which may be or not be connected to giant ELMs, and b) a gradual decline in the temperature which starts in the outer 30 cm of the plasma.

Fast SXR data was registered at sawtooth crashes allowing a detailed study of the spatial structure of the n=1 precursors. A study of the sawtooth characteristics as a function of beta was performed and will be presented in a separate publication [17]. Here we make a summary of the results and concentrate on the sawtooth collapses at the termination phase.

All sawtooth crashes, even those before the good confinement phase, were found to have clear m=n=1 precursors. For β_N~0.3-0.5, the m=n=1 precursor starts to grow 1-3 ms before the collapse and attains a large amplitude and a significant perturbation even outside the q=1 surface is observed in soft X-ray emission and electron density fluctuations. This indicates large MHD coupling between the m=1 and higher harmonics outside r(q=1). Further evidence of large MHD coupling is observed during the collapse, when a fast MHD perturbation, is observed to move outwards to radii larger than r(q=1). Further out, the typical sawtooth' heatpulse is observed with a time of arrival at the edge around 10 ms for β_N~0.5. This short heat pulse time is due to a large mixing radius, caused by the large extent of the MHD perturbation and by the large q=1 location.

For β_N~0.5, unusual precursors showing double m=n=1 structure started to be observed. For β_N>0.55 the "internal kink" mode was sometimes observed a long time before the sawtooth collapse (see Fig 3), growing exponentially in less than 100 μs before the collapse. Sawtooth collapses were found to lead to giant ELMs. A sawtooth crash in conjunction to an ELM provokes a collapse of the temperature at all radii. The plasma is usually unable to recover from these global events due to the subsequent large impurity influx [6].

At β_N~0.7 the overall sawtooth observations have all the characteristics of the limiting phenomena observed for $\beta_N \geq 1$ in low B_ϕ discharges, i.e. the m=1 oscillations observed in the SXR signals both before and during the crash extend out to the plasma edge. An ELM occurs almost immediately and there is no observable heat pulse.

A transition in the character of the post-cursor oscillations occurs for β_N~0.5. Continuous n=2 and n=3 oscillations are observed to grow just before or during a sawtooth collapse (This can be seen in Fig 1 for discharge 26087). These oscillations continue to grow for a few hundred ms after the crash. However the dominant toroidal mode number of the sawtooth post-cursor appears to depend on the phase in which the sawtooth occurred. Early sawteeth are followed by n=2 and a small

amplitude n=3. While the later sawtooth collapses at β_N>0.5 are in all cases followed by n=3 oscillations.

IVa - A SAWTOOTH DURING THE TERMINATION PHASE

Figs 6 to 8 show an analysis of SXR data for a sawtooth at β_N~0.7. Phase II, for the discharge 26076 (with B_ϕ=2.66T) is very similar to the one observed for the best D-D discharge 26087 (with B_ϕ=2.9T), i.e. a slow collapse of the outer temperature, is followed by a fast sawtooth-like collapse combined with an ELM. The observed n=1 oscillations have larger amplitudes than in the discharges shown in Fig 1, which allow us to see the MHD effects much more clear in the raw data.

Fig 6 shows a sequence of SXR brightness profiles around the sawtooth crash. The kink effect of an m=n=1 precursor is observed around the centre. This mode grows in 100 μs causing the central crash indicated in the Fig. A fast MHD perturbation propagates to the edge in 25 μs. This "instantaneous" connection between the core and the edge is followed by a giant ELM in 100 μs.

Fig 7 shows the horizontal SXR MHD oscillations observed 1.5 ms before the sawtooth crash. Surprisingly, it was found that the m=n=1 precursor has phase reversals at two different radii indicating that q(R) has to be near unity at two quite distinct radii. The central kink and the two m=1 islands are clearly seen in the tomographic reconstruction shown in Fig 8. The temperature profiles before and after the sawtooth collapse for an early sawtooth at the begining of the high performance phase and the sawtooth discussed here are shown in Fig 9. The temperature profiles around the later sawtooth (Fig 9b), show a large "flatish" region between 3.4 and 3.7m corresponding to the region where the two m=1 islands are observed in the SXR signals (Fig 8). Modelling of this MHD observation and the q-profile likely to be associated with it are presented later in section VIII.

Fig 7 shows the complexity of modes with low m/n numbers that are observed to grow in phase II. On the outer SXR channels one can see an m=2,n=1 mode with half the frequency of the central mode. This is also seen in the tomography reconstruction shown in Fig 8. Higher frequency oscillations, are likely to be n=3 with m=3-4. (The apparent central structures are an artefact of the inversion method with a restricted number of lines of sight, so that at given angles m=0 and m=2 components are intermixed).

V - SLOW TEMPERATURE COLLAPSES

In the majority of discharges the beginning of phase II coincides with a gradual temperature collapse. This is initially observed outside the q=1 region, typically within the outer 30% of the plasma. In some discharges, as in the best D-D discharge 26087 and discharge 26076 discussed in the previous section, the slow temperature fall is followed by a large sawtooth collapse combined with an ELM. In others, e.g. discharge 26095 (in Fig 1), no large sawtooth or ELM is observed in phase II. In this section we describe the observations of MHD activity at the onset and during the gradual temperature collapses.

In some of the discharges the slow magnetic signals show sudden changes in the rate of growth of low n magnetic activity. This can be seen in Figs 1 and 3 for discharge 26087. A detector of the frequency of n=1 modes shows that, as in the previous phase, the dominant n=1 activity is still from the plasma core ("internal kink" and fishbones). In the absence of fast data it is not possible to say whether outer modes are also present. In the following examples it is shown that m>1 islands, not normally observed during phase I, sometimes grow during phase II.

(i) The first example shows a slow termination phase where no large sawtooth or ELM is involved. This is a discharge similar to 26095, (but with B_ϕ=3.1 T) for which fast magnetic data was available during phase II. The overview in Fig 10 shows a sawtooth collapse and 300ms later a slow temperature collapse. Both phenomena occur for β_N~0.5. The close-up in Fig 11 shows the measured n=1 activity around the slow temperature collapse. The top signal shows fishbone bursts. The maximum fishbone amplitude decreases as the bursts develop into a continuous mode. Filtering out the frequencies of central modes ($\gtrsim$15kHz), the n=1 signal shows a burst of oscillations with frequencies around 7 kHz. As the mode starts to grow the temperature in the outer ECE channel starts to decrease while the D_α emission increases. The maximum effect on the temperature is observed at radii close to the q=2 surface, which is further inside than in the discharges discussed previously because of the higher B_ϕ. The outer collapse is followed by a sequence of small sawtooth-like crashes which bring the temperature in the centre down further. Recovery of the temperature near the edge does not occur, presumably due to the carbon influx.

(ii) Discharge 26076 (with B_ϕ=2.6 T), which was discussed in the previous section, is another example where an n=1 mode with a frequency lower than the

frequency of the central modes is observed to grow during phase II. Here, the collapse of the neutron yield coincides with a sudden growth of both the slow, outer, and the faster, central, modes. Fig 12 gives two time traces for n=1 activity, one corresponding to modes with frequencies >15 kHz, the other to the total activity. Initially only the central modes (frequencies >15 KHz) are present. At t=13.41 s a sudden increase in the amplitude of the central modes is observed (It is not clear whether this is due to a sudden growth of fishbones or to the appearance of the "internal kink".). The signal for the total n=1 activity indicates that lower frequency modes also start to grow at this time. The growth of n=1 activity precedes a flattening of the central temperature and a depression of the temperature near the edge. This is accompanied by a slow growth in the D_α emission. At the time the temperature near the edge starts to fall a frequency of 8kHz is measured with the frequency detector. The same frequency, corresponding to an m=2,n=1 mode, is later observed in the fast SXR signals (shown in Figs 7 and 8). This discharge has a lower magnetic field than most of the hot-ion H-mode discharges and consequently m>1 modes are closer to the wall and are more clearly detected with the magnetic pick-up coils.

While in the second example both central and outer modes grow during phase II, in the first example only the outer mode is observed to grow during this phase. The magnetic fluctuations, corresponding to the slow mode, measured at the wall are small, giving in both cases an estimated m=2,n=1 island size at the q=2 surface of only a few cms. It appears therefore that this mode alone is too small to have a significant effect on confinement.

VI - EDGE ACTIVITY

During JET H-modes, a typical ELM is characterised by a fast D_α spike, with a rise-time of <250 μs and duration of 1ms [18]. This is associated with disturbances in the outer 20% of the plasma observed with the multichannel reflectometer, ECE and SXR diagnostics. The decrease in the ELM repetition rate and ELM stabilisation observed during some H-modes has been associated with large values of T_e (low resistivity) close the edge [19].

In the discharges discussed here, the characteristic D_α spikes of ELMs are observed after the L-H transition. Then, they occur less often and finally disappear at the beginning of phase I (see Fig 1). However, ECE signals near the edge indicate that in these discharges edge activity is never totally stabilised. Fig 2 shows a central and an

outer ECE signal. The central signal shows the sawtooth-like effect of fishbones. The measurement from near the edge, also show a sawtooth-like effect which does not always correlate with the fishbones. The edge activity is associated to small bursts of D_α. These "mini-ELMs" are observed throughout phase I and continue to be observed during phase II. The typical repetition rate of 50-100 Hz decreases, while the observed effect on the ECE signals increases as the discharge evolves in time.

During phase II, at the time when the slow temperature collapses are observed, possible evidence for other edge activity is found in the D_α signals. Fig 13 shows fast D_α spikes observed during the slow termination in discharge 26087. This is not observed in the ECE and SXR signals indicating that they originate in a region even further out than the"mini-ELMs ". They grow in amplitude during phase II and have repetition rates in the range 0.5-1 kHz.

Both types of edge activity mentioned above are quite distinct from the giant ELMs observed at the end of phase II. Here we can distinguish two types: the large D_α spikes which are preceded by sawtooth activity, and large $D\alpha$ spikes with no clear n=1 precursor. A sawtooth combined with an ELM appears to be a high beta event (β_N>0.5). The large ELMs observed in phase III are not normally preceded by n=1 activity. It is possible that the sudden appearance of large ELMs is related to the increased impurity content, which increased the resistivity near the edge [19, 20].

In the sawtooth/ELM combination it is not clear whether the sawtooth affects the confinement right up to the last closed flux surface and the observed D_α spike is the consequence of a ballistic heat-pulse, or whether a separate edge mode could be triggered by the fast heat pulse by increasing the pressure gradient. The analysis of ballooning stability near the edge shows that prior to these global events, the edge plasma may be approaching the limiting value of the local pressure gradient for ideal instability rather than the resistive limit calculated for other large ELMs observed in JET [20].

Due to diagnostic limitation at high frequencies it not possible to obtain a consistent picture about oscillations with high mode numbers which could possibly be associated to the edge activity observed during phase II. Frequencies larger than 60 kHz corresponding to n=6-10 are normally observed at JET in ELM regimes [18]. In a couple of discharges where high frequency oscillations with 90-100 kHz were clearly observed during phase I, they appeared in bursts, with the maximum amplitude not in phase with the maximum amplitude of fishbones. It is not clear whether these

could be fishbone precursors as observed in PDX [21] or whether they could be related to the "mini-ELMs". Reflectometer data shows that high frequency activity grows in amplitude before the large ELMs observed in phase III, however it is not clear whether the same always occur before the giant ELMs observed at the end of phase II.

VII- THE D-T DISCHARGES

Within the range of frequencies studied, the MHD activity observed during phases I and II in the D-T discharges with 10% T (nos. 26147 and 26148) was found to be similar to other hot-ion H-modes.

Fig 14 shows the oscillations observed with the microwave reflectometer, close to the edge, around the neutron emission collapse for discharge 26148. The broad band region lasting ~20 ms corresponds to the giant ELM that follows the sawtooth. The sawtooth is preceded by coherent oscillations in several distinct frequencies. One notices the n=1-3 components of a fishbone burst decreasing in amplitude at 20 kHz. For the time resolution needed for the Fourier analysis it is not possible to see the growth of the "internal kink". A few other modes are observed growing 2-3 ms before the sawtooth collapse: a low frequency mode at 7 kHz, likely to be m=2,n=1; an n=3 mode with a frequency close to 60kHz, and, an independent higher frequency oscillation at around 90 kHz. After the sawtooth collapse the central plasma rotation decreases and n=1 and n=3 modes reappear with frequencies close to 1/3 of the pre-sawtooth values, in agreement with reduced plasma rotation.

Only in phase III do the two D-T discharges show some MHD activity different from the other discharges. The D_α plot for discharge 26148, in Fig 1, shows a sequence of large ELMs. Before each one of these ELMs a growing m=2,n=1 mode with a low frequency of 5kHz was observed. A Fig and description of the magnetic data can be found in reference [3]. As mentioned above, JET ELMs are not normally preceded by n=1 activity except in high beta regimes when the ELM is combined with a sawtooth crash (In this case the precursor is a central m=n=1 mode). Reference [3] showed that the evolution of the m=2, n=1 mode appear to be related to the evolution of the amplitude of alpha particle ion cyclotron emission measured near the edge. This raises the possibility of a relationship between the highly non-isotropic edge α particle velocity distribution and the observed MHD activity.

Alpha particle driven modes, such as toroidicity induced Alfven eigen-modes have predicted frequencies higher than the present diagnostic systems have allowed us to measure. Stability calculations have in any case suggested that these modes are stable [3, 5, 22].

VIII - DISCUSSION

a) MHD modelling

Although the β_N values in the high performance discharges go up to 0.8, the plasma is calculated to be stable to high-n ideal ballooning modes in the region outside the q=1 surface [23]. Only within the q=1 radius is the plasma found to be close to the ballooning stability boundary. However, in this region with q<1 unstable ballooning modes would have very large mode numbers, n > 100. These high n values are probably not relevant. At the plasma boundary, in the region $\psi > 0.95$, very large pressure gradients exist. In this region there is no ballooning limit due to the large bootstrap current at the time of maximum β [5]. The ideal MHD n=1 external kink mode is predicted to be very stable. The 'internal' kink mode is usually ignored in β limit MHD stability calculations because the influence of this mode on the β limit is very difficult to estimate from linear MHD calculations. However, at high values of β_N the 'internal' kink mode increasingly couples to the higher (m>1) poloidal harmonics and influences a larger part of the plasma.

Modelling of the n=1 precursor to the sawtooth observed at the termination of the good confinement phase has been performed using the linear resistive MHD codes CASTOR [24] and FAR [25] The objective was to simulate two main observations: the large radial extent of the modes and the double m=n=1 structure.

As discussed above, in some discharges there is direct coupling between the central sawtooth and edge MHD activity at the high performance termination. This effect requires strong coupling, in the sense that the central m=1 harmonic must couple to harmonics resonant near the edge ($m \geq 4$). Calculations show that such strong toroidal coupling occurs through either high poloidal beta or large edge current gradients associated with the bootstrap current. Both features are observed in these discharges [5]. Another factor which in these discharges contributes to large amplitudes of m>1 harmonics near the edge, is the extent of the q=1 region, which increases during phase I. (A comparison of observed inversion radii for an early sawtooth and a sawtooth in phase II is shown in Fig 9). Preliminary results of calculations using

monotonic q-profiles are shown in [26] As it will be discussed below the evolution of the central portion of the q-profiles during phase I is uncertain. Further calculations should consider the possibility of flat and non-monotonic q-profiles. Final results will be reported elsewhere [17].

The most unexpected observation is that of two m=n=1 inversions found in SXR data taken before the phase II sawtooth collapse. Fig 15 gives the result of resistive MHD modelling using the FAR code. Fig 15a gives the calculated flux surfaces of the MHD perturbation added to the equilibrium in the horizontal mid-plane corresponding to the non-monotonic q-profile shown in Fig 15b. The details of the outer portion of the q-profile and plasma shape are determined by equilibrium reconstruction, while the inner portion of the q-profile has been adjusted to match the tomography observation (Fig 8). For this calculation the measured pressure profile has been used. It can be seen that the reasonable agreement between the experiment (Fig 8) and simulation (Fig 15a) indicates a slightly non-monotonic q-profile ($q_o \lesssim 1.1$), with q=1 at two radii. If the central q value is reduced slightly ($\Delta q_o \sim 0.05$) from that shown in Fig 15(b), then the n=3 mode becomes strongly unstable; a result which appears consistent with the frequent observations of n=3 modes in phase III.

Thus the modelling of the MHD observations at the termination of the good performance, implies that the q profile is nearly flat over a very large region, with a slight magnetic shear reversal. There are a few difficulties related to this conclusion. As it will be discussed in the next section, it is difficult to understand how a non-monotonic q-profile could be established. Fast SXR data was available around the sawtooth collapses, but not during the high performance phase. Thus we do not know at what stage in the high performance phase the two m=n=1 islands have developed. For $\beta_N < 0.5$ the sawtooth precursors observed in SXR data show only one m=n=1 island, indicating that early on in the high performance phase the q-profile is likely to be monotonic with a central value below unity.

From the point of view of stability of the "internal kink" mode it is not completely understood how a non-monotonic q-profile could have been stably accessed, allowing phase I to be such a long sawtooth-free period. Ideal models [27], do not predict any evident stable route to the "internal kink" mode, which could explain sawtooth stabilisation for the high values of beta poloidal observed during phase I. Nearly flat q-profiles are predicted to be even more unstable [28]. Fast particle stabilization, is believed to stabilise the sawtooth in ion-cyclotron heating regimes [29]. On the other hand for NBI heating at JET, $\omega_{Dh}/\omega^*_i \sim (r_1/R_o)\,(E_h/T_i)$ is of the

order of unity ($r_1/R_o \sim 1/6$; $E_h \sim 140$ keV, $T_i \sim 20$-25 keV). Thus in the discharges of interest here, the fast ion injection energy does not seem to be sufficiently high to satisfy one of the requirements for fast particle stabilisation, i.e. $\omega_{Dh}/\omega^*_i > 1$ [29]. One possibility is that of combined ion viscosity and diamagnetic stabilisation [30]. It appears that the significant central diamagnetic frequencies ($\omega^*_i(r_1) \sim 5$ kHz) allied with ion-ion collisions in these discharges can stabilise the n=1 mode until $\gamma_o > \omega^*_i$.; where γ_o is the growth rate calculated for $\omega^*_i, \omega^*_e = 0$. It is also possible that the ideal m=1 modes are saturated with relatively small core displacements as suggested by the non-linear models in references [31-33], while the resistive mode is stabilised by ω^* effects until the end of phase I.

A similar problem exists on understanding how the non-monotonic q-profile is accessed relative to the n=3 mode. Calculations with the FAR code show that n=2,3 infernal modes [34] become unstable for low shear q-profiles with q~1 in the central region. Thus an evidently stable route for these modes normally not observed until phase II, is also hard to envisage; again it may be that ω^* effects may play a role.

b) Comments on the shear reversal

In order to understand how shear reversal could have been achieved, the evolution of the current density during phase I has been studied with the transport code TRANSP [35]. The effects of both NBI current drive and bootstrap current have been considered.

It is difficult to explain shear reversal simply using current drive arguments since the peaked temperature profile is calculated to give rise to a very peaked conductivity and hence a monotonic q profile with significant positive shear.

The bootstrap current, which is thought to contribute to the generation of negative shear in pellet enhanced performance (PEP) plasmas in JET [36], appears to be to small in the plasma interior of a hot-ion H mode to strongly perturb the ohmic current profile. In addition, the explanation of shear reversal in the case of PEP plasmas also relies on a broad initial current profile caused by experimenting early in the discharge (not the case for most hot-ion H modes) and the transient inversion of the temperature profile, and hence current profile, by the pellet injection. In any case the beam driven current calculated for the hot-ion H modes discussed in this paper, is peaked in the plasma centre and therefore tends to oppose the generation of negative shear.

Any rapid changes in parameters, such as the Z-effective profile, close to the time of the collapse are not expected to strongly alter the ohmic current profile in the plasma interior since the high central electron temperature gives a long resistive diffusion time.

An estimate of the possible rate of change of q_o has been obtained from TRANSP simulations for discharge 26087. The simulated q-profile was flattened inside the q=1 surface at the sawtooth at t=12.37 s (see Fig 1) and its evolution due to resistive diffusion was modelled. As the discharge evolves through phase I, q_o decreases as the current builds up in the centre. At the end of phase I, t=13.4 s, the q-profile is monotonic with a reduction of $\Delta q \sim 0.05$ in the plasma core. It is possible that current diffusion could be influenced by the magnetic islands due to the fishbone activity observed throughout phase I. This was not included in this analysis.

Within the experimental error, equilibrium calculations with the IDENTD code [37] that use magnetic and kinetic data, would allow slightly non-monotonic q-prolifes to be present throughout phase I. However, the polarimetric measurements of the internal poloidal field cannot be reconciled with such equilibria within their nominal error bars, and favours monotonic q-profiles with q_o well below unity. For high values of beta, $\beta_N > 0.5$, including the time when the two q=1 surfaces are observed in the SXR data, it has not been possible to obtain equilibrium reconstruction with the polarimeter data.

c) Comparison of observations with limiting MHD phenomena observed at the Troyon Limit

Phase II in the discharges studied here occur for values of $\beta_N > 0.5$. Overall the sawtooth observations have all the characteristics of the "beta-crashes" observed for $\beta_N \sim 1$ in low $B\phi$ discharges, i.e. both the m=1 precursor and the crash have a radial extent to the edge, a heat pulse of finite duration is not observed, and an ELM occurs almost immediately.

However, the "beta-crashes" are not associated with an irreversible collapse of β. This latter effect may be related to the high plasma energy content, leading to higher losses and easier overloading of the wall in the discharges considered here. The irreversible nature of this process is the subject of another paper [6].

In general the collapse of beta in the high beta low $B\phi$ discharges has been associated with the growth of large n=2 and n=3 modes [7,38]· Such modes are sometimes observed in phase III of the discharges studied here. However in the latter they are clearly the remnants of large sawtooth collapses, instead of being a general feature.

IX - CONCLUSIONS

JET hot-ion H modes show a rich variety of MHD activity. Some observations were found to be similar to those in high beta regimes, while others are new and appear to be pertinent to high performance discharges. Detailed mode identification during the phase of high confinement and the phase when the high performance was lost has been presented. The D-T and D-D discharges showed no difference in the MHD behaviour during the high performance and loss of high performance phases.

Fishbones are found to be the main MHD activity observed during the high confinement phase. Fishbones increase in amplitude throughout the phase of good confinement and in most discharges are found to reach similar amplitudes at the end of this phase. Early in the good confinement phase a saturation of both ion and electron temperatures profiles is observed shortly after the onset of fishbones. Further experiments and modelling are necessary to determine whether these modes play a significant role in determining the time evolution of the temperatures.
During the high confinement phase, fast ions are not sufficiently energetic to have a stabilizing influence on m=1 modes. The sawtooth-free periods observed in this phase may be due to the combined stabilization of large ion diamagnetic frequencies and ion-ion collisions [30].

During the termination of the high performance a larger variety of MHD activity is observed than in the previous phase. In some discharges the internal kink grows significantly giving rise to the striking observation of a sawtooth combined with an ELM. This global MHD event is similar to the limiting phenomenon previously observed in JET high beta discharges closer to the Troyon limit. In some discharges fishbone activity is observed to change from bursts into continuous oscilations. Outside the q=1 region, a variety of MHD oscillations is observed to grow. These include modes with an m/n ratio between 1 and 2 and edge instabilities possibly associated with much larger mode numbers.

In some discharges the end of the high performance phase is sudden and accompanied by a large MHD event such as a large ELM or a sawtooth collapse with

an extremely fast heat wave, shortly followed by an ELM. However, in the majority of discharges the termination phase does not start with a large and obvious MHD event. In some a sudden growth of low n magnetic activity is observed, but this cannot be generalized due to lack of data with high time resolution. In two discharges the slow deterioration of the electron temperature in the outer 30% of the plasma, which is a characteristic of the slow terminations, appears to start at the growth of m=2,n=1 islands. However the island sizes were found to be small and may not therefore have a large effect on confinement. During the termination phase small ELM-like spikes in the D_α emission with repetition rates 0.5-1 kHz are often observed. This behaviour might have its origin in MHD activity close to the plasma edge.

The spatial structure of the central oscillations, observed during the terminating phase is unusual. Two m=n=1 islands are found, and this suggests nearly flat, non-monotonic q profile, consistent with MHD analysis using the FAR code [25]. However, it is not clear how these profiles could have developed or at what stage during the high performance phase they were established.

ACKNOWLEDGEMENTS

We would like to thank H.P.L. de Esch for useful discusions, J. Cordey, A.Gibson, G.Cottrell and D.Campbell for comments on the text. M.F.F.Nave would like to thank LNETI and Associacao EURATOM/IST for their support during the realization of this work.

REFERENCES

[1] Thompson, E, Stork, D., de Esch, H.P.L.and the JET Team, accepted for publication in Physics of Fluids B (1993)
[2] The JET Team, Nucl. Fus. 32 (1992) 187
[3] Cottrell, G.A. et al, Nuc.Fus. 33 (1993) 1365
[4] Marcus, F. et al., Nuc.Fus. 33 (1993) 1325
[5] Balet, B. et al. , Nuc.Fus. 33 (1993) 1345
[6] Reichle, R. et al, Termination of the high performance in JET (in preparation)
[7] The JET Team (presented by P. Smeulders), Proc. of 13th IAEA Conf. on Plasma Physics and Contr. Fus. Research, Washington, vol.1 (1990) 219
[8] Stork, D. et al, Proc. 19th EPS Conf. Contr. Fusion & Plasma Phys., vol. I (1992) 339

[10] Campbell, D.J et at, Phys. Rev. Lett 60 (1988) 2148

[11] Nave, M.F.F. et al.,Proc. 19th EPS Conf. Contr. Fusion & Plasma Phys., vol. I (1992) 439

[12] Von Hellerman, M. et al., Rev. Sci. Instr., 61,3479 (1990)

[13] de Esch, H.P.L. et al. Proc 17th EPS Conf. Contr. Fusion & Plasma Physics (Amsterdam), vol I, (1990)90.

[14] Stott,P., "Review of JET diagnostics and results", Basic and Advanced Fusion Plasma Diagnostic Techniques (Proc. Course and Workshop, Varenna 1986) vol3, CEC Brussels (1987) 2148

[14a] Wesson et al, Nuc. Fus. 29 (1989) 641

[15] Coppi, B., Migliuolo, S. and Porcelli, F., Phys. Fluids 31 (1988) 1630

[16] Nave, M.F.F. et al., Nucl.Fus. 31 (1991) 697

[17] Nave, M.F.F. et al., "Limiting MHD phenomena in JET high beta discharges" (in preparation)

[18] Ali-Arshad et al., Proc. 19th EPS Conf. Contr. Fusion & Plasma Phys., vol. I (1992) 227

[19] Colton, A.L. and Porte,L., Proc. 20th EPS Conf. Contr. Fusion & Plasma Phys., vol. I (1993) 11

[20] de Blank, H.J. et al, Joint Varenna-Lausanne Workshop on Theory of Fus. Plasmas (1992) 285

[21] Strachan, J.D. et al., Nucl.Fus. 25 (1985) 863

[22] Kerner,W. et al, Proc. 20th EPS Conf. Contr. Fusion & Plsma Phys., vol. I (1993) 183

[23] Huysmans, G.T.A. and Goedbloed, J.P. "Low-n ideal and resistive MHD stability of JET discharges", FOM Rijnhuizen Report (1993)

[24] Kerner, W. et al., Proc. 18th EPS Conf. Contr. Fusion & Plasma Phys., vol. IV (1991) 89

[25] Hender,T.C., Robinson, D.C.and Snipes, J.A., in Plasma Physics and Contr. Nuc. FusionResearch (Proc. 11th Int. Conf., Kyoto,1986), IAEA Vienna, vol 1 (1987)291

[26] Nave, M.F.F. et al., Proc. 20th EPS Conf. Contr. Fusion & Plasma Phys., vol. I (1993) 191

[27] Bussac,M. N., Pellat, R., Edery,D. and Soule, J.L., Phys.Rev. Lett. 35 (1975) 1638

[28] Nave, M.F.F. and Wesson, J., Nuc. Fus. 28 (1988) 297

[29] Porcelli, F., Plasma Phys. Cntl. Fus. 33 (1991) 1601; and references within.

[30] Porcelli F. and Migliuolo, S. ,Phys. Fluids 29 (1986) 1741

[31] Avinash, K., Phys. Fl. B 2 (1990) 2373

[32] Bishop, C.M. and Cowley, S.C., Culham Lab. Report CLM P-838 (1988)

[33] Rosenbluth, M.N., Dagazian, D. and Rutherford, P.H., Phys. Fl 16 (1984) 73
[34] Manickam, J.,Pomphrey, N. and Todd A.M.M., Nucl. Fusion 27 (1987) 1461
[35] Goldston, R.J., McCune, D.C., Towner, H.H. et al., J. Comput Phys. 43 (1981) 61
[36] Hugon, M. et al , Nucl. Fusion 32 (1) (1992) 33
[37] Blum, J., Lazzaro, E., O'Rouke, J. et al , Nucl. Fusion 32 (1) (1992) 33
[38] Huysmans, G.T. et al. , Plasma Phys. and Contr. Fusion 34 (1992).487

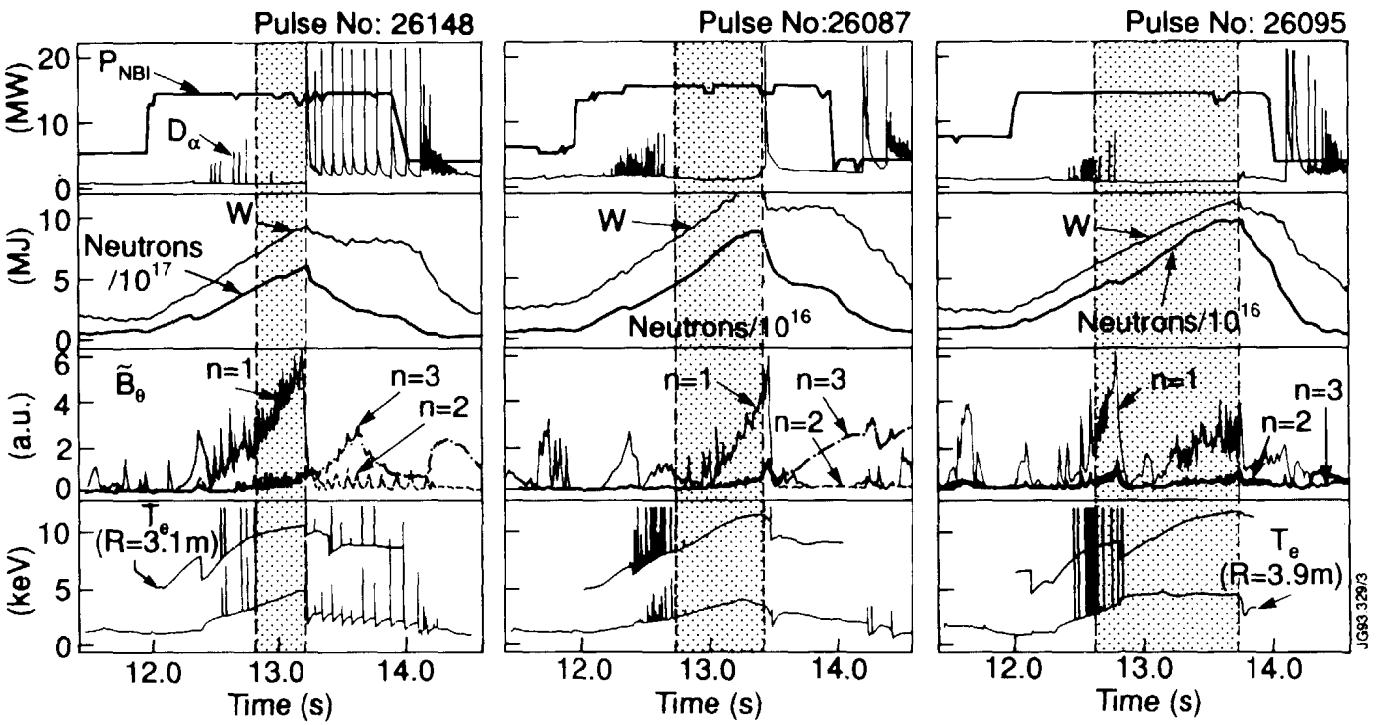

Fig.1. Time evolution of three typical high performance discharges: #26148 (D-T with 10% T, β_N^{max}=0.6), #26087 (D-D, β_N^{max}=0.8), #26095 (D-T with 0.07% T, β_N^{max}=0.75). The following traces are shown : a)NBI power and D_α emission; b) total plasma energy and total neutron rate; c) combinations of signals from magnetic pick-up coils, at 45° above the mid-plane; d) central and edge electron temperature from ECE measurements. The shaded region indicates the high confinement phase.

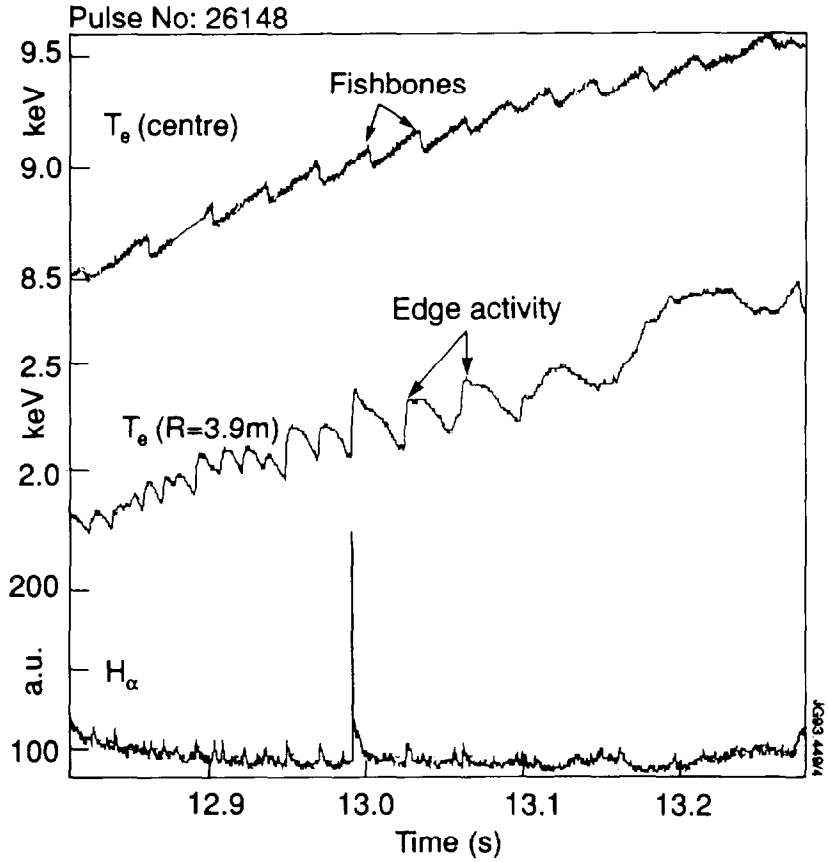

Fig.2. ECE and D_α emission signals showing central and edge effects caused by MHD activity during the high confinement phase.

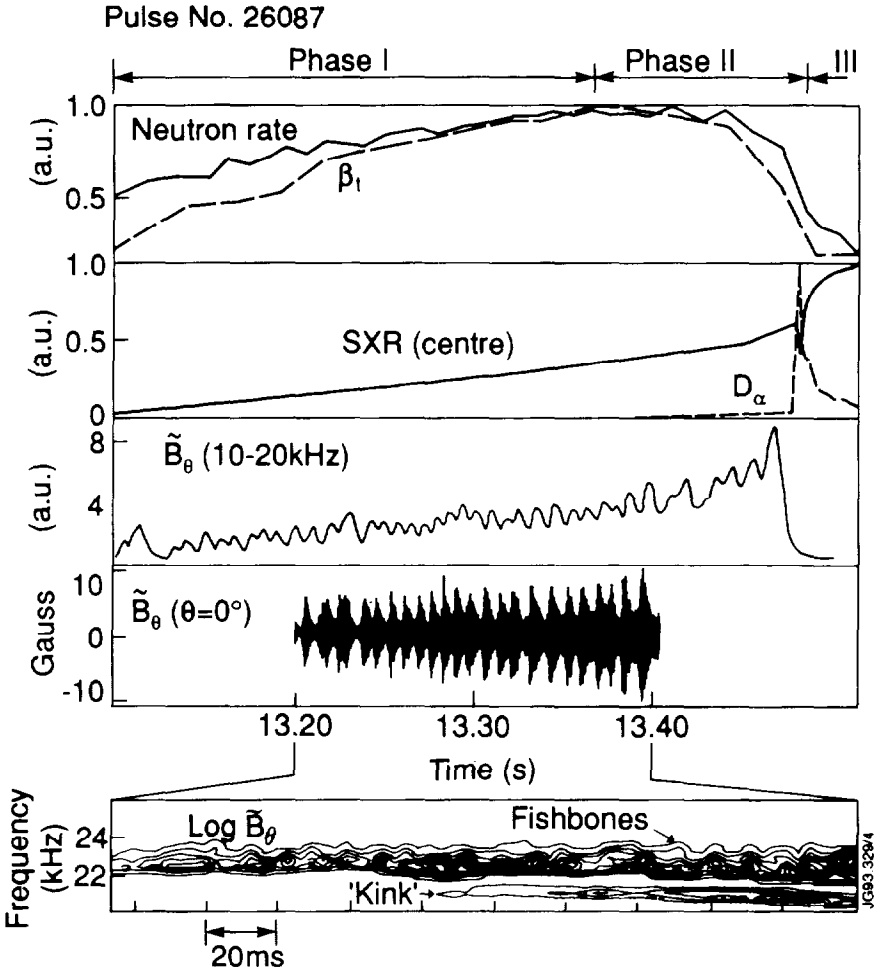

Fig.3. a) Total neutron rate and toroidal beta parameter; b) Central SXR emission and Dα emission; c) magnetic fluctuation observed with a comb filter; d) fast magnetic pick-up coil signal. The insert show the contour plot for a sequency of power spectra for the fast magnetic signal shown above.

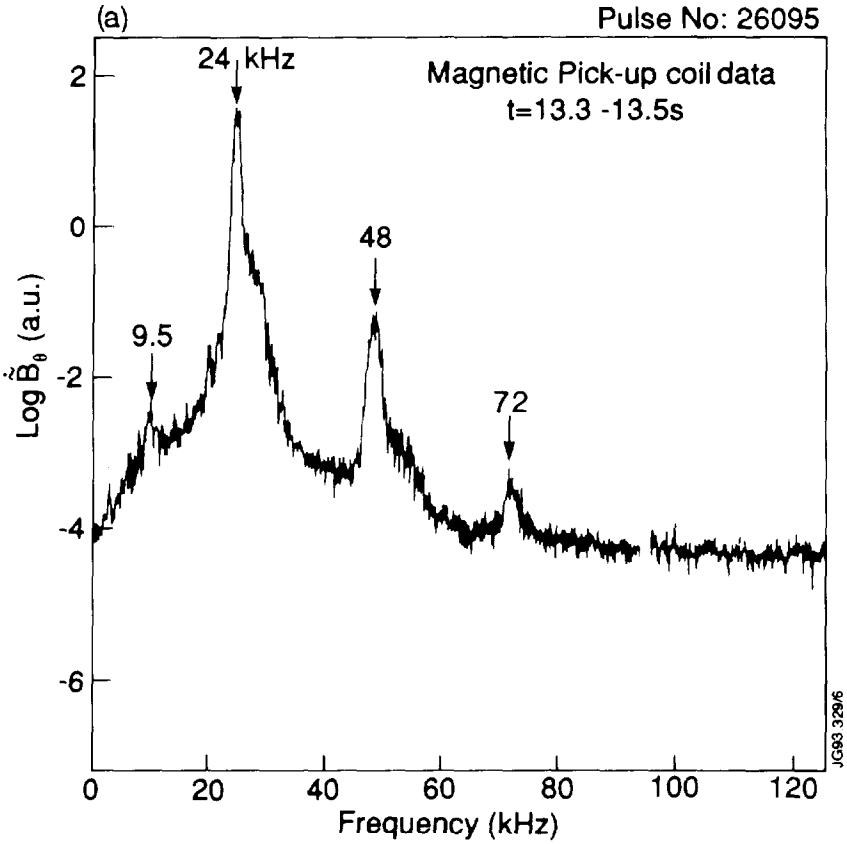

Fig.4. a) Fourier spectra of a fast pick-up coil signal (shown in Fig 5) measured during the high performance phase

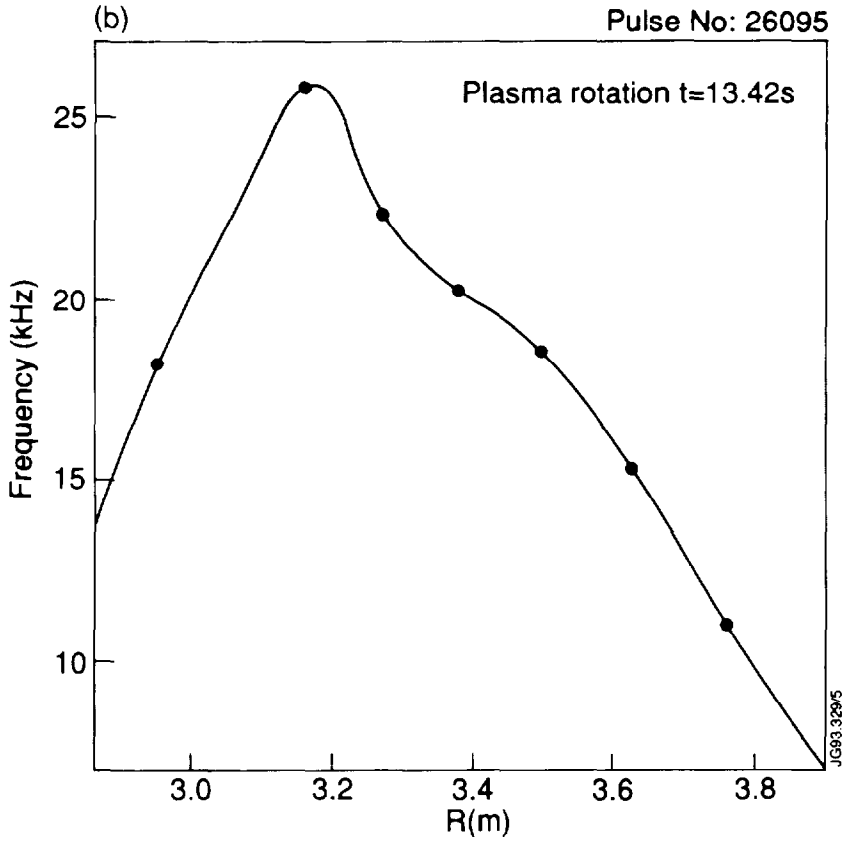

Fig.4. b) Plasma rotation profile from charge exchange measurements.

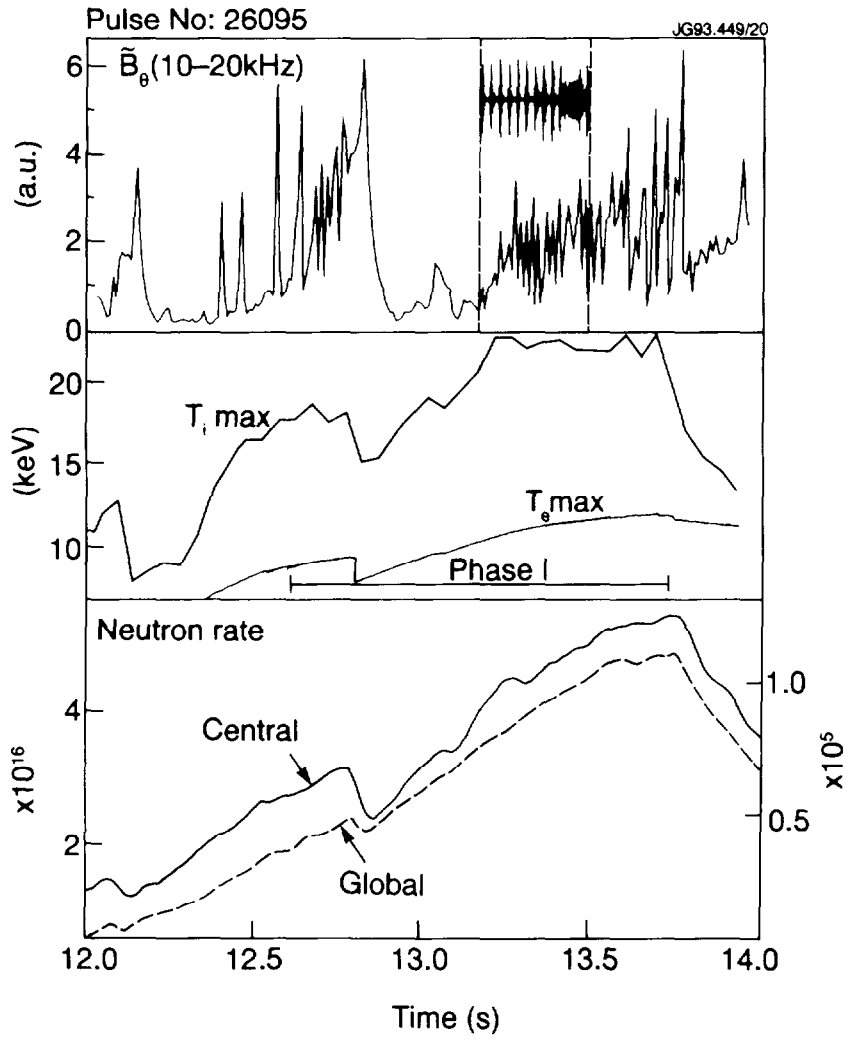

Fig.5. a) Magnetic fluctuations observed at 45^o above the mid-plane with a comb-filter (slow rms signal) and a fast magnetic magnetic signal (insert); b) central ion and electron temperatures, c) central neutron rate (smoothed) and total neutron rate.

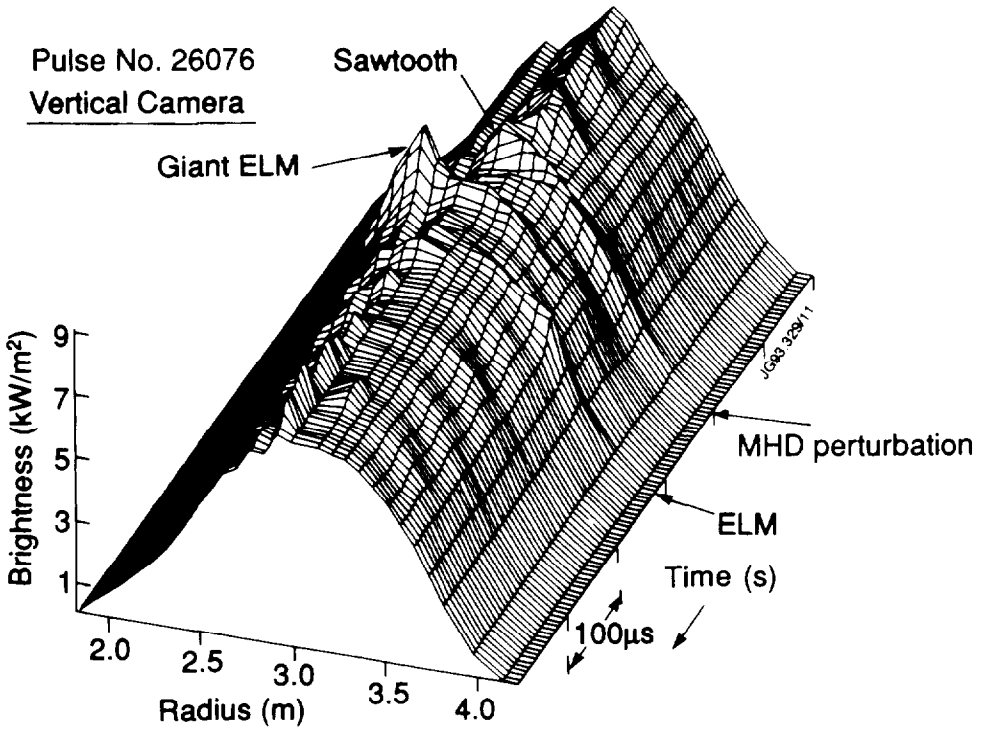

Fig.6. Sequence of SXR profiles around a sawtooth/ELM event observed during the termination of the high performance phase (at β_N~0.7).

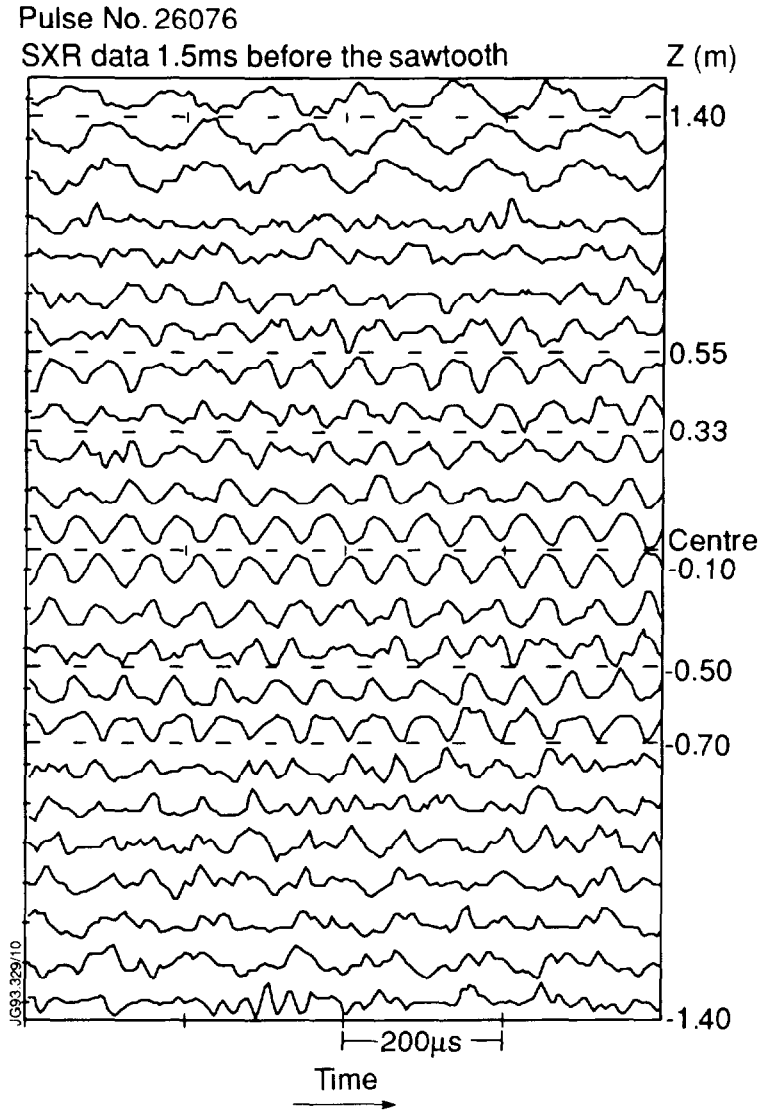

Fig.7. Precursor oscillations to the sawtooth shown in the previous Fig, observed with the SXR horizontal camera. The broken lines indicate phase reversal nodes.

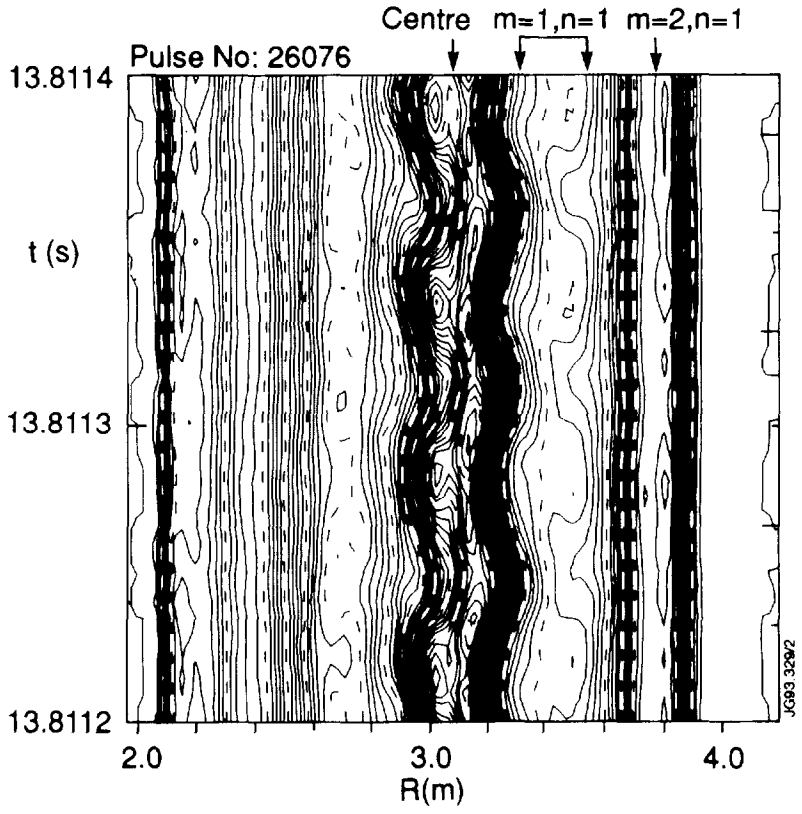

Fig.8. SXR tomography for the precursor oscillations showed in Fig 7, observed with the vertical camera It shows a double chain of m=n=1 islands, and further out a chain of m=2,n=1 islands.

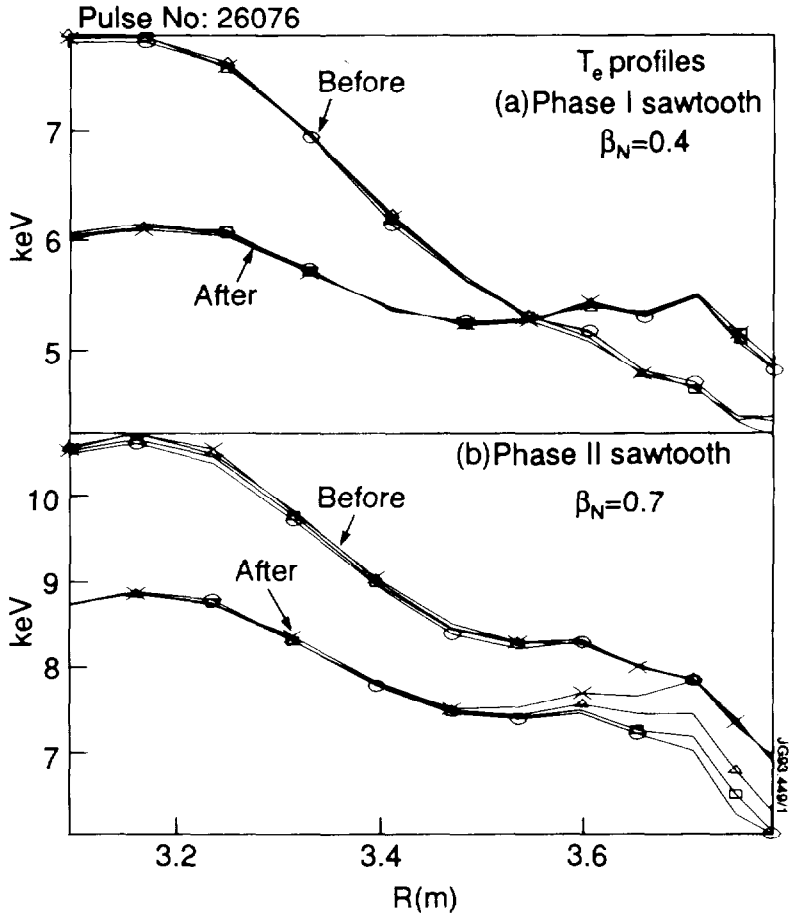

Fig.9. Temperature profiles before and after: a) an early sawtooth, and b) the sawtooth at the termination of the high performance.

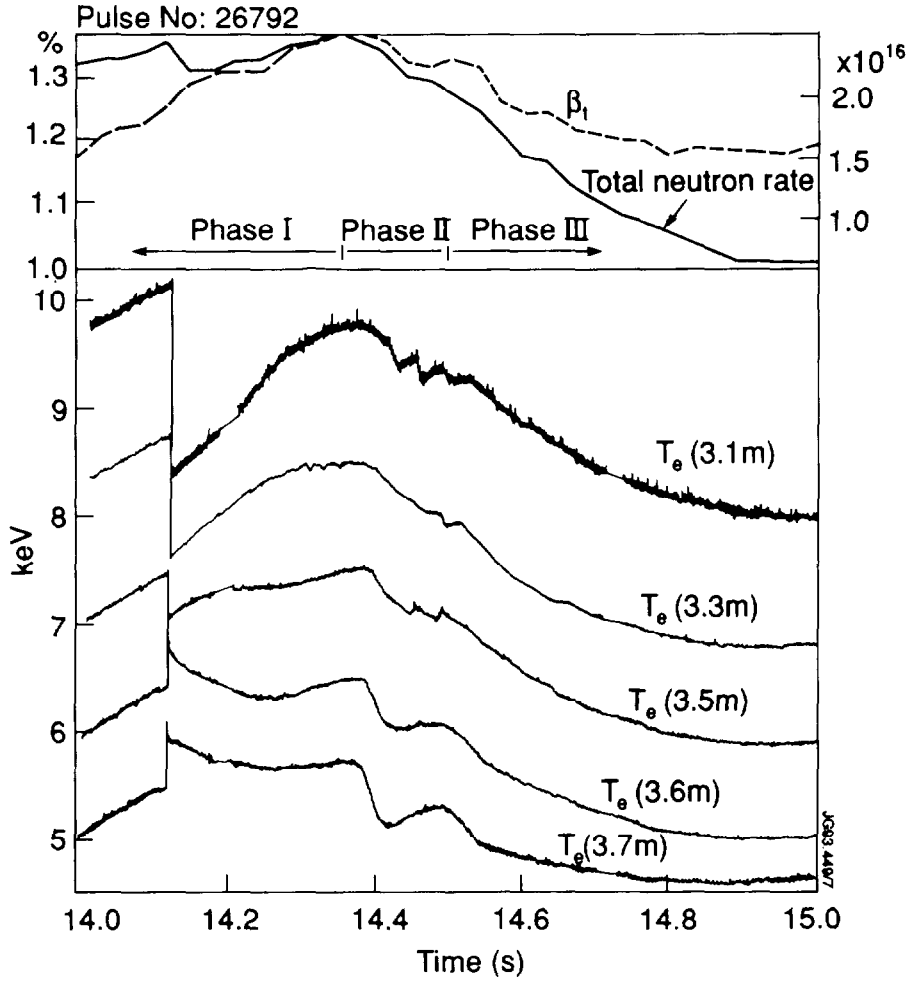

Fig.10. a) Total neutron rate and beta toroidal parameter; b) ECE signals for a discharge where the termination of the high performance coincides with a slow temperature collapse.

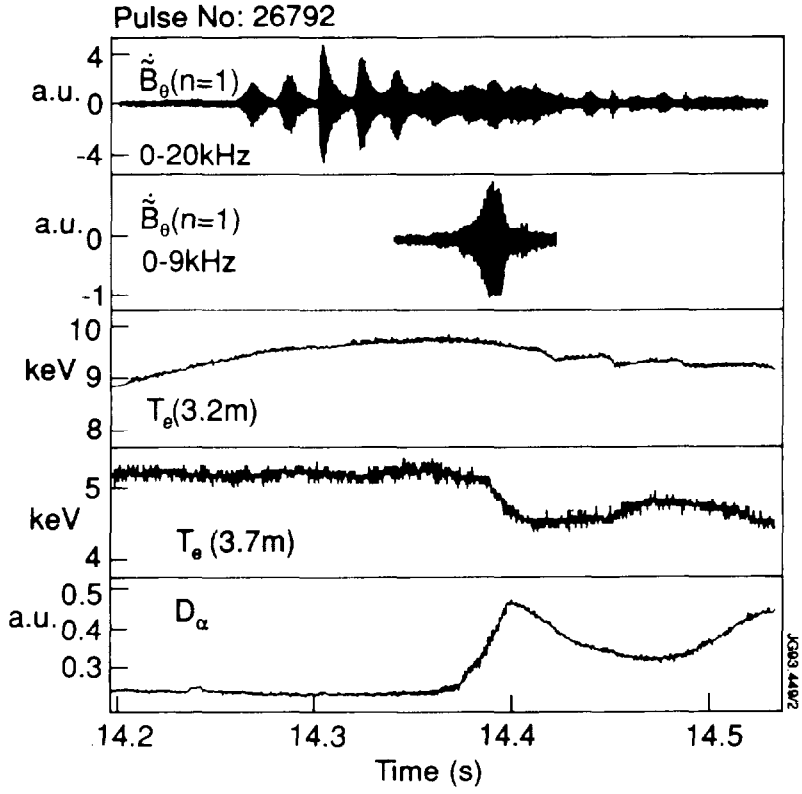

Fig.11. n=1 MHD activity observed during the slow temperature collapse. a) n=1 combination from magnetic pick-up coils; b) the n=1 signal with the central modes filtered out; c) and d) ECE traces; e) Dα emission.

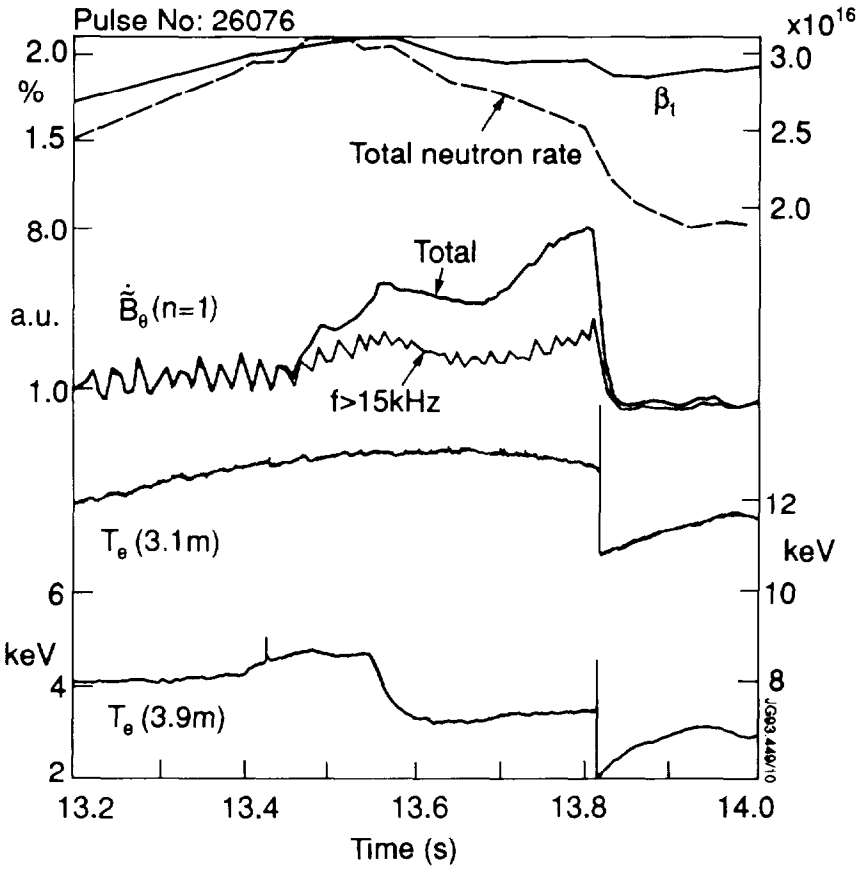

Fig.12. Time evolution of a slow temperature collapse observed before the sawtooth/ELM event described in Figs 6-9. The following traces are shown : Total neutron rate, toroidal beta parameter, total magnetic n=1 combination and n=1 combination for frequencies > 15 kHz; central and edge electron temperature.

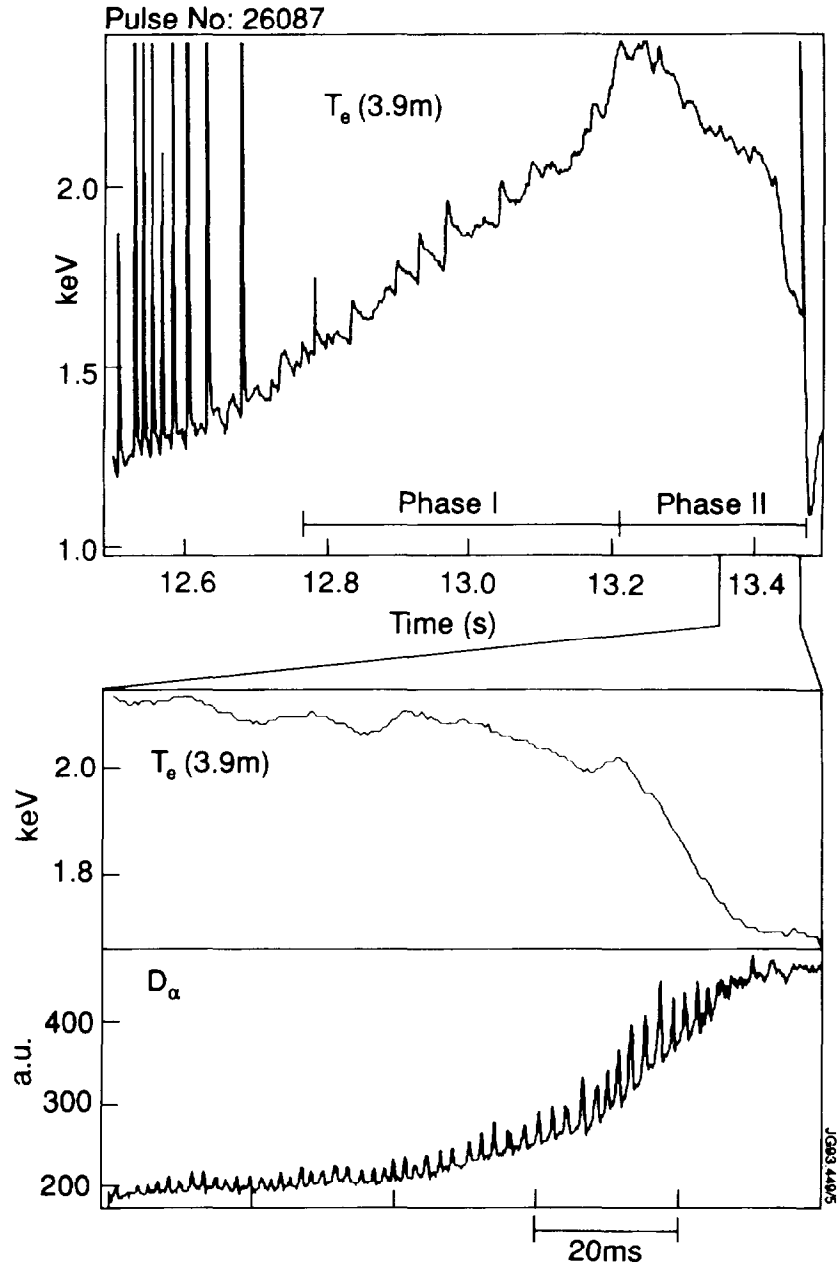

Fig.13. Edge activity observed in ECE and D_α signals during the high performance and the termination phases.

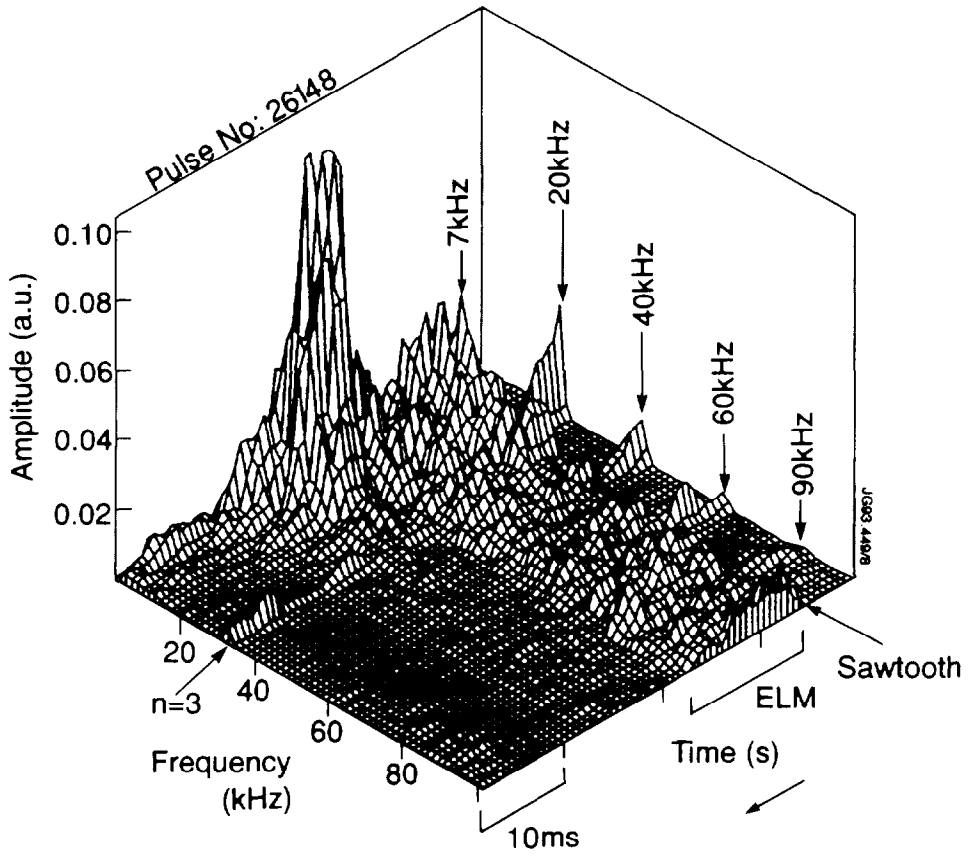

Fig.14. A sequence of power spectra from a reflectometer signal measured at R~3.8 m (n_e=2.5 x 10^{19} m^{-3}) at the termination of the high performance for one of the D-T discharges.

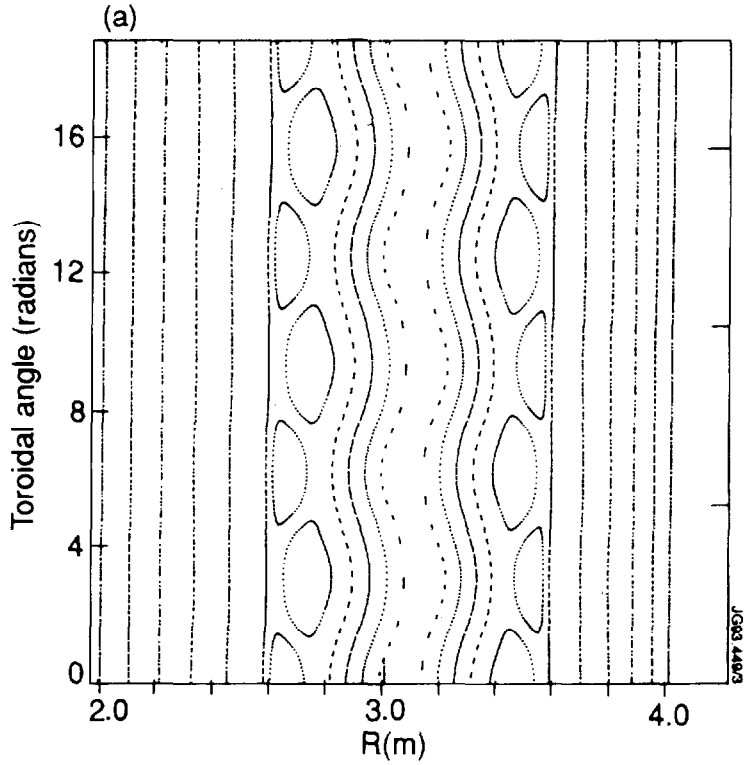

Fig.15. a) Modelling of the n=1 sawtooth precursor shown in Fig 8. Calculated flux surfaces of the n=1 perturbation added to the equilibrium in the horizontal mid-plane, showing two chains of m=n=1 islands.

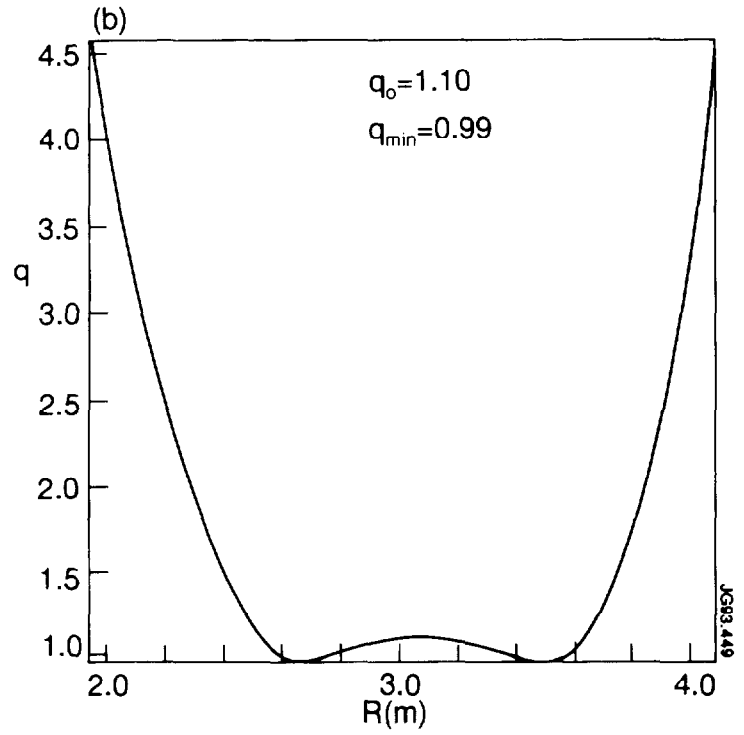

Fig.15. b) The corresponding non-monotonic q-profile.